JOURNAL OF COMPUTATIONAL PHYSICS 107, 160-175 (1993)

Global Coefficient Adjustment Method for Neumann Condition in Explicit Chebyshev Collocation Method and Its Application to Compressible Navier–Stokes Equations

JIAN-PING WANG

Department of Aeronautical Engineering, Nagoya University, Nagoya 464-01, Japan

YOSHIAKI NAKAMURA

Department of Aeronautical Engineering, Nagoya University, Nagoya 464-01, Japan

AND

MICHIRU YASUHARA

*Department of Aeronautical Engineering, Nagoya University, Nagoya 464-01, Japan**

Received October 16, 1989; revised October 27, 1992

The present paper consists of two parts. In part 1, a new technique of treating Neumann boundary conditions with an explicit Chebyshev collocation method is developed. Any Neumann boundary condition can be satisfied by adjusting all the Chebyshev coefficients of a solution, which results in a small influence on the solution and its derivatives except at the boundary. Comparisons between the new technique and several traditional ones are made for a one-dimensional advection–diffusion problem, which confirms the superiority of the new technique. The spectral accuracy of the new technique is also demonstrated. In part 2, a Chebyshev collocation code for the compressible Navier–Stokes equations is developed to solve the high-speed flows around a sphere. Good resolutions are obtained in the boundary layer by using the new technique, and comparison between the calculation and the experiment shows good agreement.

INTRODUCTION

The treatment of boundary conditions has been a significant problem in spectral methods. Since global eigenfunction expansions are used in spectral methods, solutions are more sensitive to local behavior than other numerical methods. If boundary conditions are not imposed accurately, they will produce local errors which in turn degrade the global accuracy of the solution and often lead to the onset of instability.

For periodic problems, Fourier series are used because boundary conditions are satisfied automatically and no extra process is needed. For nonperiodic problems, Chebyshev polynomials are usually utilized, and solutions can be obtained up to boundaries without taking any special measure unless the governing equation is singular there. In spite of that, the boundary conditions must be incorporated into the algorithm for solving the governing equation.

Several techniques have been proposed to treat boundary conditions in spectral methods. The most traditional one is the tau method which is characterized by expanding both the boundary conditions and the governing equation in spectral space. This method can also be recognized as an extension of the Galerkin method because the way of transforming the governing equation into spectral space is similar in both methods. So far the Chebyshev–tau method has been successfully applied to the Orr–Sommerfeld stability equation [1], the Poisson equation [2], and the incompressible Navier–Stokes equations [3].

In collocation schemes, boundary conditions can be dealt with in both physical and spectral space. In general, Dirichlet conditions are directly imposed on the solutions in physical space, whereas Neumann conditions are troublesome. Gottlieb *et al.* [4, 5] proposed the characteristic variable operating method, not only in finite difference and finite element methods, but also in spectral methods. Streett *et al.* [6] imposed Neumann conditions on the intermediate solutions of the boundary value problems in physical space. However, this led to a substantial deterioration of the convergence rate of iteration. Hussaini

* Present address: Aichi Institute of Technology, Toyoda 470-03, Japan.

0021-9991/93 $5.00

et al. [7] adjusted the highest Chebyshev coefficient to fit the Neumann condition in their explicit time-advancing Euler equations code. Furthermore, Canuto and Quarteroni [8] suggested implicit time-advancing schemes to avoid instability at boundaries. Canuto [9] also proposed an implicit treatment of boundary conditions, which can be applied to both boundary value problems and initial-boundary value ones. At internal boundaries Patera's spectral element method [10] gives good solutions for incompressible flows.

So far our study has focused on developing spectral schemes for high-speed flows which have been rarely treated with spectral methods. This is due to a strong non-linearity which makes the shock wave and boundary conditions more difficult to treat. The calculation of supersonic flows around a cylinder was carried out by Hussaini *et al.* [7] for the two-dimensional Euler equations. We [11, 12] also performed the calculations of flows around a sphere and the forward part of a shuttle-like body by solving the three-dimensional Euler equations written in generalized coordinates. In order to calculate viscous flows, we developed a code to solve the axisymmetric compressible Navier–Stokes equations [13, 14]. More recently, Kopriva *et al.* [15] succeeded in well-converged solutions on blunt body problems.

In all our previous work, the treatment of Neumann conditions has been a difficult problem. Our early treatment aimed at preventing the divergence of solution due to the propagation of errors at boundaries. In particular, when solving viscous high-speed flows, resolution of the boundary layer has a close relation to the treatment of boundary conditions. Therefore, it is required to develop a simple, accurate, and stable method to treat Neumann conditions.

In the present paper, we introduce a new technique of treating Neumann conditions for explicit Chebyshev collocation methods. The contents are divided into two parts. In part 1, a one-dimensional advection–diffusion problem is chosen as a test problem to verify the present method, where the principle of our new technique is explained, and its effectiveness is shown by comparing between the new technique and the traditional ones. In part 2, the algorithm of solving the compressible Navier–Stokes equations for high-speed flows around a sphere is described and the application of the new technique to this code is discussed.

PART 1. ONE-DIMENSIONAL ADVECTION-DIFFUSION PROBLEM

1.1. Relations between Boundary Conditions and Chebyshev Coefficients

Consider the Chebyshev expansion of a solution $u(x, t)$ written as

$$u(x, t) = \sum_{n=0}^{N} \hat{u}_n(t) \cos n\alpha, \tag{1}$$

where $\hat{u}_n$ is the coefficient of expansion, N is the number of truncated terms, and

$$x = -\cos\alpha \qquad (0 \leqslant \alpha \leqslant \pi,\ -1 \leqslant x \leqslant 1). \tag{2}$$

The first and second spatial derivatives can also be expressed likewise as

$$u_x(x, t) = \sum_{n=0}^{N} \hat{u}_n^{(1)}(t) \cos n\alpha, \tag{3}$$

$$u_{xx}(x, t) = \sum_{n=0}^{N} \hat{u}_n^{(2)}(t) \cos n\alpha, \tag{4}$$

where there are the recurrence relations between the coefficient $\hat{u}_n$, $\hat{u}_n^{(1)}$, and $\hat{u}_n^{(2)}$,

$$\begin{aligned} &C_n \hat{u}_n^{(1)} = \hat{u}_{n+2}^{(1)} + 2(n+1)\,\hat{u}_{n+1} \qquad (0 \leqslant n \leqslant N-1), \\ &\hat{u}_N^{(1)} = \hat{u}_{N+1}^{(1)} = 0, \end{aligned} \tag{5}$$

$$\begin{aligned} &C_n \hat{u}_n^{(2)} = \hat{u}_{n+2}^{(2)} + 2(n+1)\,\hat{u}_{n+1}^{(1)} \qquad (0 \leqslant n \leqslant N-1), \\ &\hat{u}_N^{(2)} = \hat{u}_{N+1}^{(2)} = 0, \end{aligned} \tag{6}$$

with

$$C_n = \begin{cases} 2 & n = 0 \text{ or } N, \\ 1 & 1 \leqslant n \leqslant N-1. \end{cases} \tag{7}$$

Then, the following equations are derived from Eq. (1) at the boundaries $x = -1$ and 1,

$$u(-1, t) = \sum_{n=0}^{N} \hat{u}_n(t), \tag{8}$$

$$u(1, t) = \sum_{n=0}^{N} (-1)^n \hat{u}_n(t), \tag{9}$$

$$u_x(-1, t) = -\sum_{n=0}^{N} n^2 \hat{u}_n(t), \tag{10}$$

$$u_x(1, t) = -\sum_{n=0}^{N} (-1)^{n+1} n^2 \hat{u}_n(t). \tag{11}$$

These give the relations between the boundary values in physical space and the coefficients in Chebyshev space, in which each boundary is composed of $N+1$ coefficients. By means of them, a number of methods of dealing with boundary conditions have been proposed. These relations are differently treated, depending on implicit and explicit schemes. In implicit schemes, they are incorporated into the system of equations, so that the resulting coefficients exactly satisfy

both the governing equations and the boundary conditions [1]. In contrast, boundary conditions are separated from the process of solving the governing equations in explicit schemes, and the solutions or the coefficients should be modified at each time step so as to satisfy the boundary conditions after integrating the governing equations [7].

1.2. Test Problem

In order to simply discuss explicit schemes, we take up the following one-dimensional advection–diffusion problem:

$$u_t + u_x = u_{xx}. \tag{12}$$

A Fourier sine series with exponentially convergent coefficients is set as the initial condition:

$$u(x, 0) = \sum_{m=1}^{M} e^{-m} \sin m\pi x. \tag{13}$$

Note that M is independent of N in Eq. (1), and throughout the present calculations, M is set to 16.

If the Neumann condition

$$u_x(-1, t)_{\text{exact}} = \sum_{m=1}^{M} m\pi e^{-(m\pi)^2 t - m} \cos m\pi(-1-t) \tag{14}$$

and the Dirichlet condition

$$u(1, t)_{\text{exact}} = \sum_{m=1}^{M} e^{-(m\pi)^2 t - m} \sin m\pi(1-t) \tag{15}$$

are satisfied at the two boundaries, $x = -1$ and 1, respectively, the exact solution becomes

$$u(x, t)_{\text{exact}} = \sum_{m=1}^{M} e^{-(m\pi)^2 t - m} \sin m\pi(x-t). \tag{16}$$

The solution is composed of various waves which converge to zero when $t \to \infty$.

There exist at least two spectral methods to explicitly solve this problem: the collocation method and the tau method, which will be discussed in the following subsections. For time integration, the first-order explicit Euler method is utilized in both methods. Before introducing our new technique, we first discuss two traditional techniques of treating Neumann boundary conditions in collocation methods.

1.3. Traditional Treatment of Boundary Conditions in Collocation Methods

The Chebyshev collocation method is characterized by discretizing the spatial coordinate x as

$$x_j = -\cos(\pi j/N) \qquad (0 \leqslant j \leqslant N). \tag{17}$$

Thus Eq. (1) becomes

$$u(x_j, t) = \sum_{n=0}^{N} \hat{u}_n(t) \cos \frac{\pi n j}{N}, \tag{18}$$

where the Chebyshev coefficients are expressed by

$$\hat{u}_n(t) = \frac{2}{C_n N} \sum_{j=0}^{N} \frac{1}{C_j} u(x_j, t) \cos \frac{\pi n j}{N} \qquad (0 \leqslant n \leqslant N). \tag{19}$$

Equations (3) and (4) for the spatial derivatives of the solution can also be discretized in the same fashion with Eq. (18), and the partial differential equation (12) is integrated in terms of time.

Since the solutions are obtained in physical space, the Dirichlet condition of Eq. (15) can be directly imposed at every time step, namely

$$u^{new}(1, t) = u(1, t)_{\text{exact}}, \tag{20}$$

where the superscript "new" indicates the value after adjustment of the boundary condition.

On the other hand, the imposing of the Neumann condition needs more elaboration. The simplest way usually used in finite difference methods is to extrapolate the solution up to the boundary. The first-order extrapolation at $x = -1$ is represented as

$$u^{\text{new}}(-1, t) = u^{\text{old}}(x_1, t) - (x_1 - x_0)\, u_x(-1, t)_{\text{exact}}. \tag{21}$$

Obviously Eq. (21) has a second-order error of $o[(x_1 - x_0)^2]$, and the new boundary value is determined locally. This kind of extrapolation works well in the present problem but frequently breaks down for highly unstable problems, for example, the high-speed flow problem described in Part 2.

The second way is to force Eq. (10) to satisfy the Neumann condition in Chebyshev space. However, unlike implicit schemes, the coefficients cannot be determined uniquely without any additional condition. Hussaini *et al.* [7] proposed a method in their supersonic inviscid flow code, where the coefficient of the highest wave number is adjusted. This procedure can be applied to the present problem as

$$\hat{u}_N^{\text{new}}(t) = -\left[u_x(-1, t)_{\text{exact}} + \sum_{n=0}^{N-1} n^2 \hat{u}_n^{\text{old}}(t) \right] \Big/ N^2. \tag{22}$$

This method introduces a local error in Chebyshev space and in turn yields a global error in physical space. Suppose that the adjusted quantity is

$$\Delta\hat{u}_N(t) = \hat{u}_N^{\text{new}}(t) - \hat{u}_N^{\text{old}}(t), \tag{23}$$

then the alteration of the solution in physical space is

$$\Delta u(x, t) = \Delta \hat{u}_N(t) \cos N\alpha. \tag{24}$$

The spatial distribution of $\Delta u(x, t)/\Delta \hat{u}_N(t)$ is illustrated in Fig. 1, where the solid circles indicate the values at collocation points. It is seen that the alteration has the same magnitude at each collocation point. Since each coefficient, which is multiplied by the square of its wave number n (see Eqs. (10) and (11)), contributes to u_x at the boundaries, adjusting the coefficient of the highest wave number leads to a smaller adjusted quantity than any one of the other modes. It should be noted that the alteration also occurs in the spatial derivatives, which will be discussed in the next subsection.

1.4. Global Coefficient Adjustment Method

A more accurate method comes from the following consideration: if the Neumann condition is imposed only by changing the boundary value, its influence may be restricted to the neighborhood of the boundary. For this purpose, we first see what will happen when the solution at the boundary is adjusted by a small quantity $\Delta u(-1, t)$ as

$$u^{\text{new}}(-1, t) = u^{\text{old}}(-1, t) + \Delta u(-1, t). \tag{25}$$

From Eq. (19), the new coefficients become

$$\hat{u}_n^{\text{new}}(t) = \hat{u}_n^{\text{old}}(t) + \frac{1}{C_n N} \Delta u(-1, t) \qquad (0 \leqslant n \leqslant N). \tag{26}$$

This implies that all the coefficients are shifted by the same quantity $\Delta u(-1, t)/N$, which becomes half of that when $n = 0$ or N. Transforming Eq. (26) to physical space by means of Eq. (1), we have an expression in physical space,

$$u^{\text{new}}(x, t) = u^{\text{old}}(x, t) + \Delta u(x, t), \tag{27}$$

where

$$\Delta u(x, t) = \frac{\Delta u(-1, t)}{N} \sum_{n=0}^{N} \frac{1}{C_n} \cos n\alpha. \tag{28}$$

The distribution of $\Delta u(x, t)/\Delta u(-1, t)$ is illustrated in Fig. 2. Note that it has a largest value at the left boundary, and converges to zero toward the right boundary. Moreover, it vanishes at all the collocation points, except at the left boundary.

We can take advantage of this characteristic to treat Neumann boundary conditions. If the coefficients, $\hat{u}_n^{\text{old}}$ are already known, they can be adjusted in the form of Eq. (26) so as to satisfy the Neumann condition (Eq. (10)), namely

$$-\sum_{n=0}^{N} n^2 \left[\hat{u}_n^{\text{old}}(t) + \frac{1}{C_n N} \Delta u(-1, t) \right] = u_x(-1, t)_{\text{exact}}. \tag{29}$$

Consequently, the unknown value of $\Delta u(-1, t)$ is obtained from this relation. Then the adjustments are performed in both Chebyshev and physical spaces, but separately. The coefficients themselves are adjusted according to Eq. (26), while the solutions are altered just by adding $\Delta u(-1, t)$ at the left boundary. Note that it is not necessary to obtain

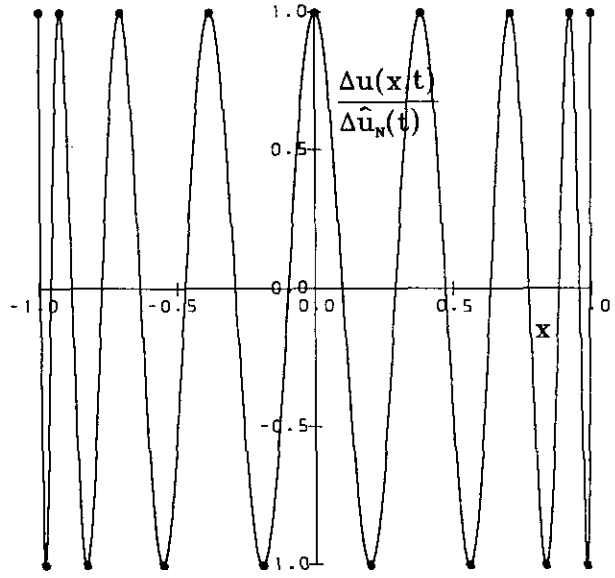

FIG. 1. Spatial distribution of $\Delta u(x, t)/\Delta \hat{u}_N(t)$ by the highest coefficient adjustment method for $N = 16$.

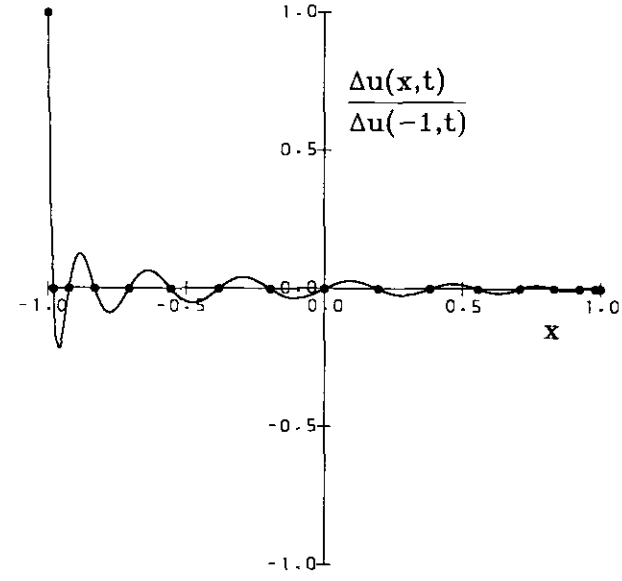

FIG. 2. Spatial distribution of $\Delta u(x, t)/\Delta u(-1, t)$ by the global coefficient adjustment method for $N = 16$.

the physical space solution by transforming the adjusted coefficients and that the adjusted coefficients are in a straightforward way used in the next step computation. This makes the algorithm compact and saves much cpu time. We call this the *global coefficient adjustment method.*

Incidentally, a similar procedure can also be taken if it is necessary to satisfy the Neumann boundary condition at the right boundary. The expressions corresponding to Eqs. (26) and (29) at $x = 1$ are written as

$$\hat{u}_n^{\text{new}}(t) = \hat{u}_n^{\text{old}}(t) + \frac{(-1)^n}{C_n N} \Delta u(1, t) \qquad (0 \leqslant n \leqslant N), \tag{30}$$

$$-\sum_{n=0}^{N} (-1)^{n+1} n^2 \left[\hat{u}_n^{\text{old}}(t) + \frac{(-1)^n}{C_n N} \Delta u(1, t) \right] = u_x(1, t)_{\text{exact}}. \tag{31}$$

Let us sum up the differences of enforcing boundary conditions with the highest coefficient adjustment method and the global coefficient adjustment method, when the same quantity $\Delta u(-1, t)$ is adjusted in both methods. Comparing Figs. 1 and 2, the former has alterations on a solution at all the collocation points, while the latter has no change at those points except at the left boundary. Furthermore, the former method can give an accurate Neumann condition at the left boundary, but the error in u_x of the same quantity appears at the right boundary due to a sharp slope there, although u_x does not change at internal collocation points since it has a peak value there. It is also obvious from these figures that the errors of the second derivative with the former method are much larger than those of the latter method. Moreover, both the first and second derivatives are less influenced in the latter method as the right boundary is approached.

1.5. Tau Method

For comparison with the collocation method, we will demonstrate the tau method in this subsection. Substituting Eqs. (1), (3), and (4) into Eq. (12), we have

$$\frac{d\hat{u}_n(t)}{dt} + \hat{u}_n^{(1)}(t) = \hat{u}_n^{(2)}(t). \tag{32}$$

This equation is integrated in terms of time to get the coefficients $\hat{u}_n$ $(0 \leqslant n \leqslant N-2)$ at the new time step. The remaining two coefficients of the highest and second-highest wave numbers, $\hat{u}_N$ and $\hat{u}_{N-1}$ are utilized to satisfy the boundary conditions, which are calculated by solving the following system of equations:

$$-(N-1)^2 \hat{u}_{N-1}^{\text{new}}(t) - N^2 \hat{u}_N^{\text{new}}(t) = u_x(-1, t)_{\text{exact}} + \sum_{n=0}^{N-2} n^2 \hat{u}_n^{\text{old}}(t), \tag{33}$$

$$-\hat{u}_{N-1}^{\text{new}}(t) + \hat{u}_N^{\text{new}}(t) = u(-1, t)_{\text{exact}} - \sum_{n=0}^{N-2} (-1)^n \hat{u}_n^{\text{old}}(t). \tag{34}$$

This method induces errors in the coefficients of the highest two wave numbers, which result in global errors in physical space. The influence of change in the coefficient of the highest wave number, $\hat{u}_N$ on the solution was discussed previously. In the same way, we define for $\hat{u}_{N-1}$

$$\Delta\hat{u}_{N-1}(t) = \hat{u}_{N-1}^{\text{new}}(t) - \hat{u}_{N-1}^{\text{old}}(t), \tag{35}$$

which alters the physical solution by

$$\Delta u(x, t) = \Delta\hat{u}_{N-1}(t) \cos(N-1)\alpha. \tag{36}$$

The distribution of $\Delta u(x, t)/\Delta\hat{u}_{N-1}(t)$ is illustrated in Fig. 3. While $\Delta u(x, t)/\Delta\hat{u}_N(t)$ is an even function in terms of x, $\Delta u(x, t)/\Delta\hat{u}_{N-1}(t)$ is an odd one. Therefore, in many cases, they can be properly combined to accurately satisfy both left and right boundary conditions.

An important difference between the collocation method and the tau method is that the former includes spatial discretizing errors unlike the latter. Therefore, the number of collocation points in the former method may affect comparison between them. Another remark should be made here; that is, the tau method will lose its usefulness for complicated multi-dimensional compressible flow problems, where the collocation method does itself justice.

1.6. Results

In this subsection, we discuss the results obtained with the abovementioned methods, and we first examine the dis-

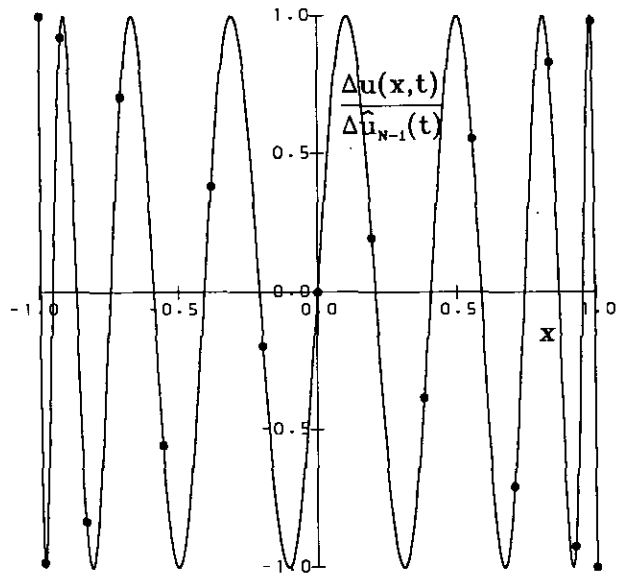

FIG. 3. Spatial distribution of $\Delta u(x, t)/\Delta\hat{u}_{N-1}(t)$ by the tau method for $N = 16$.

TABLE I

Errors at Collocation Points for $N = 16$

x	-1	-0.924	-0.707	0	0.707	0.924	1
u_x	3.74(−2)	2.16(−2)	3.43(−2)	2.03(−1)	3.43(−2)	2.16(−2)	3.74(−2)
u_{xx}	−6.26(0)	2.20(−1)	2.10(−1)	1.93(−15)	−2.10(−1)	−2.20(−1)	6.26(0)

cretizing error of the collocation method. In Tables I and II the errors of the first and second derivatives u_x and u_{xx} for the initial values at seven collocation points are listed for $N = 16$ and 32, respectively. It is seen that the worst accuracy of u_x occurs at the center, $x = 0$, where the collocation points are coarsely distributed. In contrast, the worst accuracy of u_{xx} occurs at the two boundaries, $x = -1$ and 1, whose errors are considerably larger than those at internal points. The reason for this is that the second derivative needs more information from both directions, which is difficult to satisfy at boundaries. Therefore, in our collocation algorithm, the boundary values at each time-step are imposed directly from boundary conditions without integrating the governing equation up to the boundaries.

Next we compare the accuracy of the three techniques by the collocation method: the first-order extrapolation method, the highest coefficient adjustment method, and the global coefficient adjustment method. The computations are at first performed for the collocation number $N = 16$, and a time increment $\Delta t = 10^{-5}$ is chosen to be so small that the accuracy is not influenced by it. Those results are referred to as Cases I, II, and III, respectively.

Since the test problem has an unsteady convergent solution, it is necessary to examine the time variation of accuracy. Figures 4 to 6 correspond to Cases I, II, III, respectively. The abscissa indicates the time-step number, while the ordinate represents two different quantities on logarithmic scale: average error and adjusted quantity. The thick line is the time history of the average error, defined as

$$\bar{u}_{\text{error}}(t) = \sqrt{\int_{-1}^{1} [u(x, t) - u(x, t)_{\text{exact}}]^2 \, dx}. \tag{37}$$

The thin line shows the time history of the absolute value of adjusted quantity, namely,

$$|\Delta u(-1, t)| = |u^{\text{new}}(-1, t) - u^{\text{old}}(-1, t)|. \tag{38}$$

TABLE II

Errors at Collocation Points for $N = 32$

x	-1	-0.924	-0.707	0	0.707	0.924	1
u_x	4.98(−4)	2.87(−4)	4.54(−4)	2.70(−3)	4.54(−4)	2.87(−4)	4.98(−4)
u_{xx}	−3.39(−1)	2.92(−3)	2.77(−3)	−5.18(−15)	−2.77(−3)	−2.92(−3)	3.39(−1)

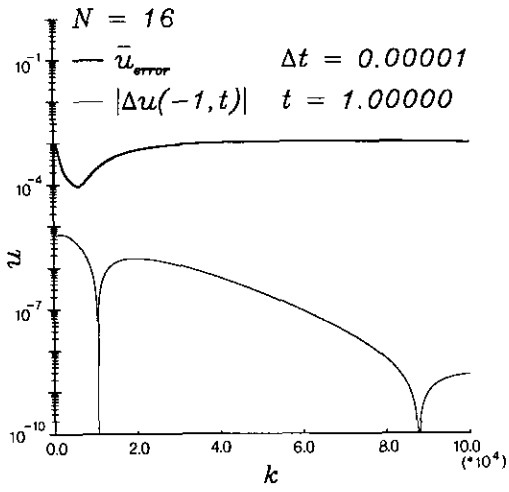

FIG. 4. Time histories of average error and absolute value of adjusted quantity for the first-order extrapolation method: $N = 16$ and $\Delta t = 10^{-5}$.

Note that for the highest coefficient adjustment method, it becomes

$$|\Delta u(-1, t)| = |\hat{u}_N^{\text{new}}(t) - \hat{u}_N^{\text{old}}(t)|. \tag{39}$$

Sudden decreases in the value of the thin line are due to the change in sign.

Comparing the thin lines, which are the adjusted values, they show the same behavior and have roughly the same magnitudes of order. On the other hand, the thick lines, namely the average errors, are remarkably different. In the early stage the accuracy of Case I is better than that of Case II, but this is reversed after approximately $t = 0.5$. Case I shows almost a constant value, while Case II decreases as time goes on. The average error of Case III

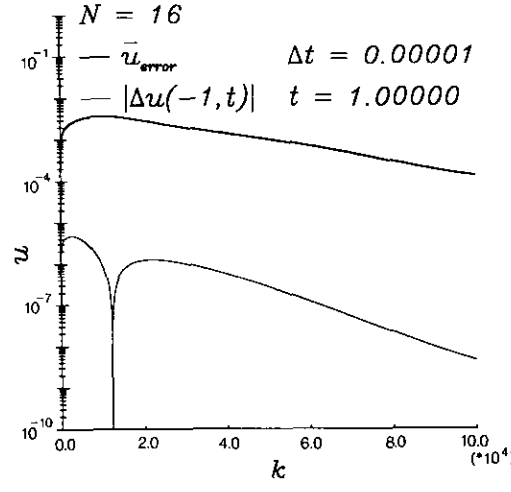

FIG. 5. Time histories of average error and absolute value of adjusted quantity for the highest coefficient adjustment method: $N = 16$ and $\Delta t = 10^{-5}$.

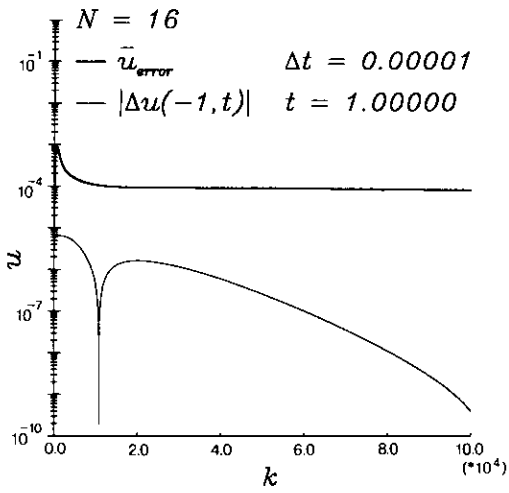

FIG. 6. Time histories of average error and absolute value of adjusted quantity for the global coefficient adjustment method: $N=16$ and $\Delta t=10^{-5}$.

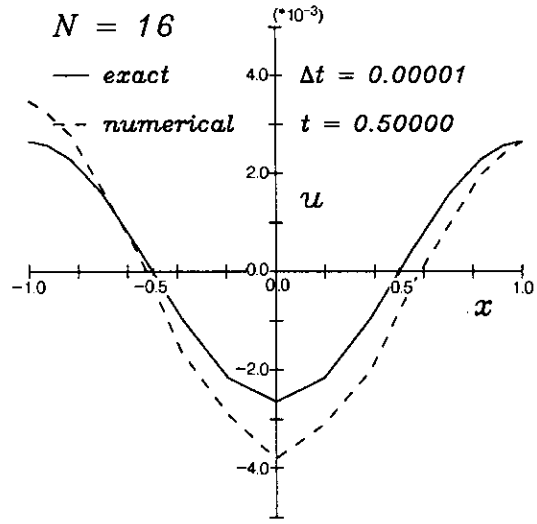

FIG. 8. Spatial distributions of numerical and exact solutions at $t=0.5$ for the highest coefficient adjustment method: $N=16$ and $\Delta t=10^{-5}$.

maintains the same level after a decrease at the beginning and is lower than those of Cases I and II. At $t=1$, the errors of Cases II and III are very close. Thus the superiority of Case III is obvious at least up to $t=1$.

The spatial error distributions at $t=0.5$ are shown in Figs. 7 to 9, corresponding to Cases I, II, and III, respectively. The solid line shows the exact solution, and the dashed line shows the numerical solution. In Case I, there exist large displacement errors, and the errors in Case II include an amplification of wave. The average error of Case III, however, is about one order of magnitude smaller as compared with the former two cases.

These results show an excellent property of the global coefficient adjustment method. However, it is not yet answered whether this method maintains the spectral accuracy. To examine this, the number of collocation points is increased from $N=16$ to 32, and the time increment is reduced to $\Delta t=10^{-7}$, which is sufficiently small to keep the converged behavior of errors. Since the cpu time and data storage are limited, we just make a comparison between the above-mentioned three techniques up to $t=0.1$, which are referred to as Cases IV, V, and VI, respectively. As shown in Fig. 10, the average error of the extrapolation method takes low values at first, and then increases, approaching the level of Case I in Fig. 4. For the highest coefficient adjustment method, the errors in Fig. 11 have the same order of magnitude with Case II in Fig. 5; that is, the accuracy was not improved by increasing the number of collocation

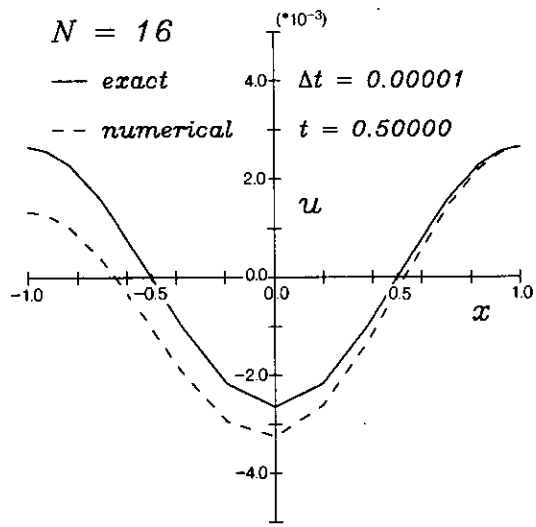

FIG. 7. Spatial distributions of numerical and exact solutions at $t=0.5$ for the first-order extrapolation method: $N=16$ and $\Delta t=10^{-5}$.

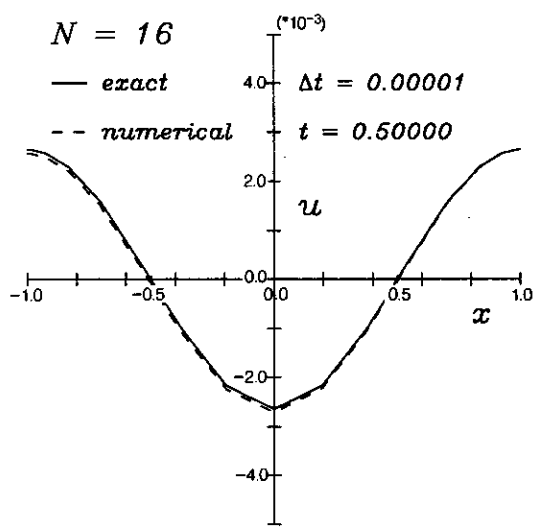

FIG. 9. Spatial distributions of numerical and exact solutions at $t=0.5$ for the global coefficient adjustment method: $N=16$ and $\Delta t=10^{-5}$.

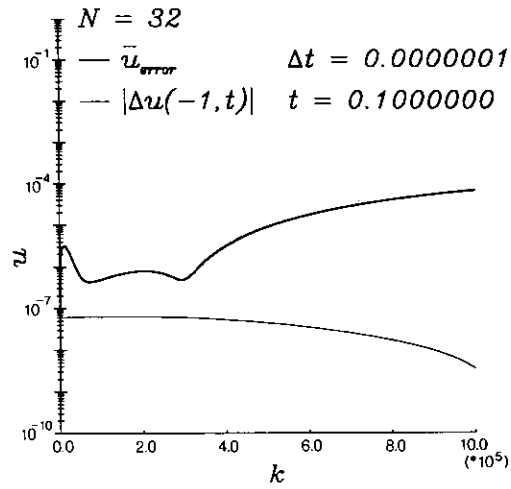

FIG. 10. Time histories of average error and absolute value of adjusted quantity for the first-order extrapolation method: $N = 32$ and $\Delta t = 10^{-7}$.

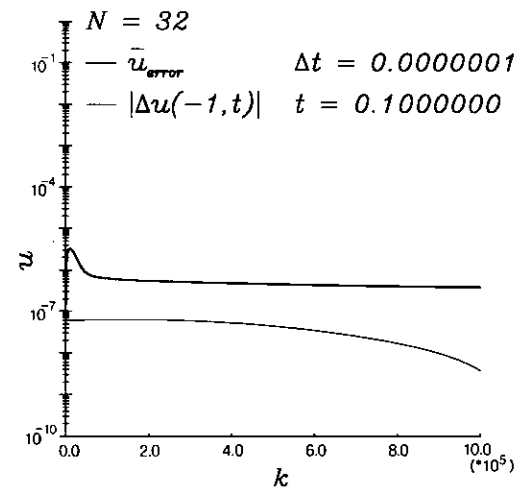

FIG. 12. Time histories of average error and absolute value of adjusted quantity for the global coefficient adjustment method: $N = 32$ and $\Delta t = 10^{-7}$.

points and decreasing the time increment. Therefore, both the extrapolation method and the highest coefficient adjustment method cannot be considered to maintain spectral accuracy. In contrast, the accuracy of Case VI in Fig. 12 is much better than the former two cases and is two orders of magnitude lower than Case III in Fig. 6.

Furthermore, in order to examine the influence of time increment, we calculated Cases VII and VIII with the global coefficient adjustment method for $N = 16$. The time increment is set to 10^{-5} and 10^{-7}, for which results are shown in Figs. 13 and 14, respectively. Comparing Figs. 12 to 14, the following key issues are found: (1) the adjusted quantity is in proportion to the time increments; (2) the error for a given number of collocation points does not change if the time increment is sufficiently small; (3) the error is affected not by the adjusted quantity but by the number of collocation points; and (4) the average error is reduced more than two orders of magnitude by doubling the number of collocation points. These characteristics verify that the spectral accuracy is obtained in the global coefficient adjustment method.

Finally, we compare the tau method explained in Subsection 1.5 with the collocation method. Figures 15 and 16 show the results for the tau method with the truncation term number $N = 16$ and 32, which are denoted as Cases IX and X, respectively. Since the tau method has two degrees of freedom in coefficients: $\Delta\hat{u}_{N-1}$ and $\Delta\hat{u}_N$, their time histories are also plotted as two thin lines.

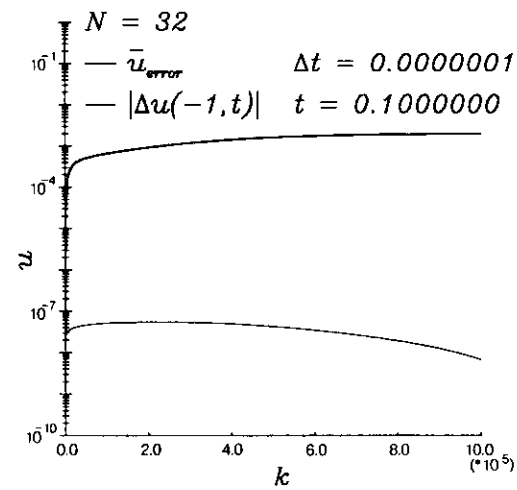

FIG. 11. Time histories of average error and absolute value of adjusted quantity for the highest coefficient adjustment method: $N = 32$ and $\Delta t = 10^{-7}$.

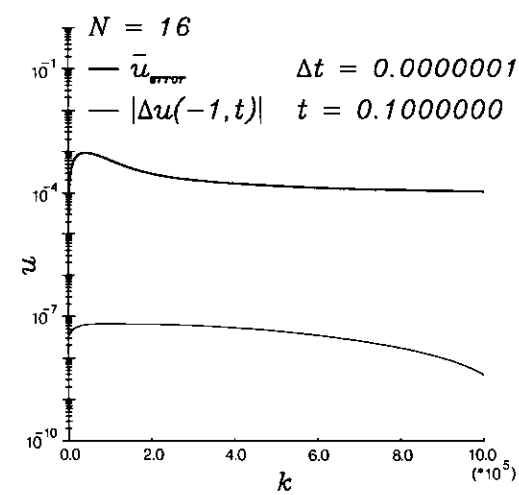

FIG. 13. Time histories of average error and absolute value of adjusted quantity for the global coefficient adjustment method: $N = 16$ and $\Delta t = 10^{-7}$.

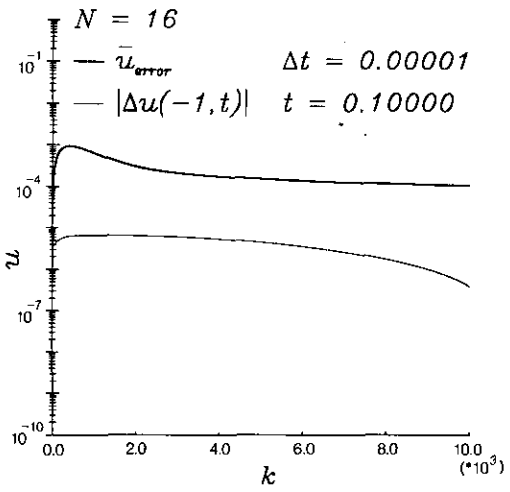

FIG. 14. Time histories of average error and absolute value of adjusted quantity for the global coefficient adjustment method: $N = 16$ and $\Delta t = 10^{-5}$.

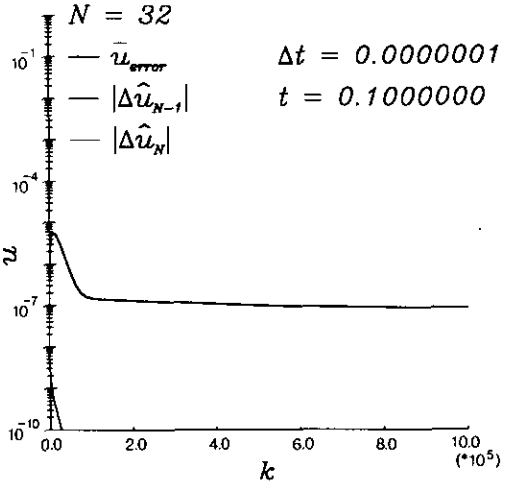

FIG. 16. Time histories of average error and absolute value of adjusted quantity for the tau method: $N = 32$ and $\Delta t = 10^{-7}$.

In regard to the average errors, Cases IX and X are worse at first than Cases III (Fig. 6) and VI (Fig. 12), but become better after a short time. It is noted that the adjusted quantities of the tau method decrease more quickly. The reason for this is as follows: Since the time integration of Eq. (32) considers the effects at boundaries, and, furthermore, the solution converges to zero, the adjusted quantities determined by Eqs. (33) and (34) may become extremely small. In contrast, discretizing errors exist in the collocation method, and the solution at $x = -1$ is obtained by the global coefficient adjustment method, instead of the time integration of Eq. (12) there. Thus, the adjusted quantities may have the same order of magnitude of variations as those at internal collocation points.

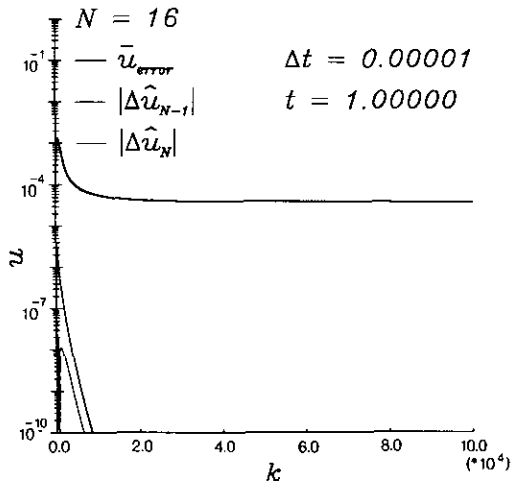

FIG. 15. Time histories of average error and absolute value of adjusted quantity for the tau method: $N = 16$ and $\Delta t = 10^{-5}$.

PART 2: APPLICATION TO VISCOUS HIGH SPEED FLOWS

2.1. Governing Equations

In order to calculate the high-speed flows around a sphere, the following axisymmetric compressible Navier–Stokes equations written in spherical coordinates are utilized:

$$Q_t + E_r + F_\theta + S = 0, \tag{40}$$

$$Q = \begin{bmatrix} \rho \\ \rho u \\ \rho v \\ e_i \end{bmatrix}, \qquad E = \begin{bmatrix} \rho u \\ \rho u^2 - \sigma_{rr} \\ \rho vu - \sigma_{r\theta} \\ e_i u - \kappa T_r \end{bmatrix},$$

$$F = \begin{bmatrix} (1/r)\,\rho v \\ (1/r)\{\rho uv - \sigma_{\theta r}\} \\ (1/r)\{\rho v^2 - \sigma_{\theta\theta}\} \\ (1/r)\{e_i v - (1/r)\,\kappa T_\theta\} \end{bmatrix},$$

$$S = \begin{bmatrix} \rho(2u + v\cot\theta)/r \\ \{\rho(2u^2 + uv\cot\theta - v^2) - 2\sigma_{rr} \\ \quad - \sigma_{\theta r}\cot\theta + \sigma_{\theta\theta} + \sigma_{\phi\phi}\}/r \\ \{\rho(3uv + v^2\cot\theta) - 3\sigma_{r\theta} \\ \quad - \sigma_{\theta\theta}\cot\theta + \sigma_{\phi\phi}\cot\theta\}/r \\ \{e_i(2u + v\cot\theta) - 2\kappa T_r - (1/r)\cot\theta\,\kappa T_\theta\}/r \\ \quad + (1/\gamma)\,p\nabla\cdot\mathbf{v} - \Phi \end{bmatrix},$$

where ρ, p, T, and e_i are density, pressure, temperature, and internal energy per unit volume, respectively, r, θ, and ϕ are the spherical coordinates, and the subscripts r, θ, and ϕ

represent derivatives with respect to those values. $\mathbf{v}$ is the velocity vector, whose radial and tangential components are u and v, respectively; γ is the ratio of specific heats.

The relations between sresses and strain rates are defined as

$$\begin{aligned}
\sigma_{rr} &= -(1/\gamma)\, p + 2\mu\{u_r - \tfrac{1}{3}\nabla\cdot\mathbf{v}\},\\
\sigma_{\theta\theta} &= -(1/\gamma)\, p + 2\mu\{(1/r)\, v_\theta + u/r - \tfrac{1}{3}\nabla\cdot\mathbf{v}\},\\
\sigma_{\phi\phi} &= -(1/\gamma)\, p + 2\mu\{u/r + v\cot\theta/r - \tfrac{1}{3}\nabla\cdot\mathbf{v}\},\\
\sigma_{r\theta} &= \sigma_{\theta r} = \mu\{v_r + (1/r)\, u_\theta - v/r\},
\end{aligned} \tag{41}$$

where

$$\nabla\cdot\mathbf{v} = u_r + (1/r)\, v_\theta + (2u + v\cot\theta)/r. \tag{42}$$

The dissipation function is

$$\begin{aligned}
\Phi = \mu[&2u_r^2 + 2\{(1/r)\, v_\theta + u/r\}^2\\
&+ (u/r + v\cot\theta/r)^2\\
&+ \{v_r + (1/r)\, u_\theta - v/r\}^2\\
&- \tfrac{2}{3}\{\nabla\cdot\mathbf{v}\}^2].
\end{aligned} \tag{43}$$

The viscosity coefficient μ is approximately calculated by Sutherland's formula

$$\mu = \mathrm{Re}^{-1}\, M_\infty\, T^{3/2}(1 + C/T_\infty)/(T + C/T_\infty), \tag{44}$$

where $C = 120$ K and $T_\infty = 288.15$ K, Re is the Reynolds number, and M_∞ is the Mach number of the free stream. The thermal conductivity κ is given as

$$\kappa = (\gamma - 1)^{-1}\, \mathrm{Pr}^{-1}\, \mu, \tag{45}$$

where Pr is the Prandtl number, and is set to 0.72 in the present study. The pressure is calculated from the internal energy, assuming a calorically perfect gas, as

$$p = \gamma(\gamma - 1)\, e_i. \tag{46}$$

In addition to the above equations, the state equation is necessary to calculate the temperature

$$T = p/\rho. \tag{47}$$

In the above equations each quantity is made non-dimensional by the corresponding reference values: the length r_b, the density ρ_∞, the pressure $(1/\gamma)\,\rho_\infty a_\infty^2$, the temperature T_∞, the internal energy $\rho_\infty a_\infty^2$, the velocity a_∞, the viscosity coefficient $\rho_\infty r_b a_\infty$, and the thermal conductivity $(\gamma - 1)\,\rho_\infty a_\infty r_b c_p$. Here r_b denotes the radius of a sphere, a is the speed of sound, c_p is the specific heat at constant pressure, and the subscript ∞ denotes the values in a free stream.

2.2. Coordinate Transformation

A shock-fitting technique is applied in the present study to treat the shock wave, where the shock wave is regarded as a boundary which goes on moving until convergence is reached. Thus, the computational region is confined between the shock wave and the body surface in the radial direction and between the axis of symmetry and the downstream boundary in the tangential direction. Moretti's transformation [16] is used to have a square computational region,

$$\begin{aligned}
X &= (r - r_b)/\{r_s(\theta, t) - r_b\},\\
&\qquad (r_b \leqslant r \leqslant r_s,\ 0 \leqslant X \leqslant 1),\\
Y &= (\pi - \theta)/\theta_{\max},\\
&\qquad (\pi - \theta_{\max} \leqslant \theta \leqslant \pi,\ 0 \leqslant Y \leqslant 1),
\end{aligned} \tag{48}$$

where r_s is the radial coordinate of shock wave, and $\theta_{\max}$ is the angle between the axis of symmetry and the downstream boundary and is set to 80° in the present study. Incidentally, θ is an angle from the x axis which is the same direction as the main stream. Therefore, $\theta = \pi$ points to the upstream.

The metrics are derived from Eq. (48) as follows:

$$\begin{aligned}
&X_r = [r_s(\theta, t) - r_b]^{-1}, \qquad X_\theta = -XX_r r_{s,\theta},\\
&X_t = -XX_r r_{s,t},\\
&Y_r = 0, \qquad Y_\theta = -(\theta_{\max})^{-1}, \qquad Y_t = 0.
\end{aligned} \tag{49}$$

These metrics are constants or can be easily calculated, except that $r_{s,\theta}$ is calculated by the one-dimensional Chebyshev spectral method.

Suppose that $Q(r, \theta, t)$ is a solution variable in Eq. (40); then its spatial derivatives can be transformed to those with regard to X and Y coordinates as

$$Q_r = Q_X X_r, \qquad Q_\theta = Q_X X_\theta + Q_Y Y_\theta, \tag{50}$$

where Q_X and Q_Y are calculated by the two-dimensional Chebyshev collocation method.

2.3. Two-Dimensional Chebyshev Collocation Method

The global function $Q(X, Y, t)$ is expanded by the Chebyshev polynomials as

$$Q(X, Y, t) = \sum_{n=0}^{N} \sum_{m=0}^{M} \hat{Q}_{mn}(t) \cos m\alpha \cos n\beta, \tag{51}$$

where $M+1$ and $N+1$ are the numbers of collocation points in the X and Y directions, respectively. α and β are related to X and Y through

$$\begin{aligned} X &= (1-\cos\alpha)/2 \qquad (0 \leqslant \alpha \leqslant \pi,\ 0 \leqslant X \leqslant 1), \\ Y &= (1-\cos\beta)/2 \qquad (0 \leqslant \beta \leqslant \pi,\ 0 \leqslant Y \leqslant 1). \end{aligned} \tag{52}$$

Then the spatial derivatives are obtained by using inverse transforms as follows:

$$\begin{aligned} Q_X(X, Y, t) &= -2 \sum_{n=0}^{N} \sum_{m=0}^{M} \hat{Q}_{mn}^{(1,0)}(t) \cos m\alpha \cos n\beta, \\ Q_Y(X, Y, t) &= -2 \sum_{n=0}^{N} \sum_{m=0}^{M} \hat{Q}_{mn}^{(0,1)}(t) \cos m\alpha \cos n\beta. \end{aligned} \tag{53}$$

The coefficients $\hat{Q}_{mn}^{(1,0)}(t)$ and $\hat{Q}_{mn}^{(0,1)}(t)$ have recurrence relations with $\hat{Q}_{mn}(t)$ in the same fashion as Eq. (5),

$$\begin{aligned} C_m \hat{Q}_{mn}^{(1,0)} &= \hat{Q}_{(m+2)n}^{(1,0)} + 2(m+1)\hat{Q}_{(m+1)n} \\ &\qquad (0 \leqslant m \leqslant M-1), \\ \hat{Q}_{Mn}^{(1,0)} &= \hat{Q}_{(M+1)n}^{(1,0)} = 0, \\ C_n \hat{Q}_{mn}^{(0,1)} &= \hat{Q}_{m(n+2)}^{(0,1)} + 2(n+1)\,\hat{Q}_{m(n+1)} \\ &\qquad (0 \leqslant n \leqslant N-1), \\ \hat{Q}_{mN}^{(0,1)} &= \hat{Q}_{m(N+1)}^{(0,1)} = 0, \end{aligned} \tag{54}$$

where

$$\begin{aligned} C_m &= \begin{cases} 2 & m = 0 \text{ or } M, \\ 1 & 1 \leqslant m \leqslant M-1, \end{cases} \\ C_n &= \begin{cases} 2 & n = 0 \text{ or } N, \\ 1 & 1 \leqslant n \leqslant N-1. \end{cases} \end{aligned} \tag{55}$$

For discretization, the collocation points are defined by

$$\begin{aligned} X_i &= \{1-\cos(\pi i/M)\}/2 \qquad (i = 0, 1, \ldots, M), \\ Y_j &= \{1-\cos(\pi j/N)\}/2 \qquad (j = 0, 1, \ldots, N), \end{aligned} \tag{56}$$

where M and N are chosen to be integers of two raised to the nth power. The coefficients $\hat{Q}_{mn}$ and the spatial derivatives Q_X and Q_Y are calculated by using the fast Fourier transform (FFT).

All of the spatial derivatives included in Eq. (40) are transformed to the form of Eq. (50) and calculated by the spectral collocation method. Operations other than spatial derivatives are performed in physical space.

For the time integration of the governing equation,

$$Q_t + LQ = 0, \tag{57}$$

an explicit predictor–corrector scheme [8] is utilized as

$$\begin{aligned} \tilde{Q} &= (1 - \Delta t\, L^k)\, Q^k, \\ Q^{k+1} &= \tfrac{1}{2}[Q^k + (1 - \Delta t\, L)\tilde{Q}], \end{aligned} \tag{58}$$

where the superscript k denotes the value at the kth time step.

2.4. Boundary Conditions

The body surface is regarded as a non-slip and adiabatic wall: $u = v = p_X = T_X = 0$. The conditions for symmetry are imposed at the axis of symmetry ($Y = 0$), $v = u_Y = p_Y = e_Y = 0$. Since the flow is supersonic at the downstream boundary except near the wall, the solutions there are determined by its upstream properties. Accordingly it is not necessary to explicitly impose the boundary conditions, and the values at the boundary can be calculated in the same fashion as those at the internal grid points.

The shock wave surface is a moving boundary, and its initial location is given as a parabola in the present study, which should be set properly to prevent divergence of the solution. The shock-fitting technique [18] is composed of two stages. The first stage is to move the shock wave, using the solutions at a new time-step. The moving speed of the shock wave V_s is determined by the relation

$$V_s = \sqrt{(p_2 - 1)/\{(1 - 1/\rho_2)\gamma\}} - |\mathbf{u}_{1n}|. \tag{59}$$

where $|\mathbf{u}_{1n}|$ is the component of free-stream velocity normal to the shock wave, and the subscript two denotes values immediately downstream of the shock wave. The second stage is performed after moving the shock wave to a new location. The boundary conditions immediately downstream of the shock wave are calculated by the Rankine–Hugoniot relations.

With regard to the above-mentioned boundary conditions, the Dirichlet conditions are directly imposed on the solutions, while the Neumann conditions are given by the global coefficient adjustment method discussed in Part 1. The extension from one-dimensional to two-dimensional problems is straightforward because each Neumann condition can be enforced one-dimensionally. To avoid repetition, the Neumann conditions are not imposed in the Y direction at the two grid points where the body and the shock wave intersect with the axis of symmetry.

2.5. Filtering

Filters are used in the spectral collocation methods to damp the amplification of high frequency disturbances, like the artificial viscosity in the finite difference method. The differences between them are: (1) the former has a global effect but the latter has a local one; (2) the former is imposed

in spectral space but the latter, in physical space. Since aliasing errors occur and nonlinear waves are always produced and propagate between the body surface and the shock wave, it is necessary to filter solutions in order to keep them smooth and prevent the onset of instability.

The filtering operation in the present code is expressed as

$$Q(X, Y, t) = \sum_{n=0}^{N} \sum_{m=0}^{M} \sigma(m)\, \sigma(n)\, \hat{Q}_{mn}(t) \cos m\alpha \cos n\beta, \tag{60}$$

where σ is a smoothing function which is unity at lower frequencies and tends to zero toward higher ones. In this paper, the modified form of the raised cosine filter [17] is used, which is defined by

$$\sigma(m) = \begin{cases} 1 & (m \leqslant m_c). \\ \frac{1}{2}\{1 + \cos[\pi(m - m_c)/(M - m_c)]\} & \\ & (m_c < m \leqslant M). \end{cases} \tag{61}$$

This smoothing function changes gradually from one to zero when m is larger than m_c, so that the strength of smoothing is controlled by the critical frequency m_c. Generally it is not necessary to filter the solutions at every time-step if the amplification of disturbance does not grow too fast. The filtering process is significantly associated with accuracy and stability. If the time interval of filtering is too long or the filter is too weak, the instability will occur. Conversely if the time interval of filtering is too short or the filter is too strong, the accuracy will deteriorate. This is a contradiction, and in order to have a stable solution, the accuracy has to be sacrificed to some extent.

2.6. Results

In the present study, we applied the spectral collocation method to solve the viscous high-speed flows around a sphere, and we performed the computations on the FACOM VP-200 vector computer. Since there exist rapid changes in the temperature and velocity distributions in the boundary layer, more elaboration is needed to obtain good accuracy for viscous flows than is needed for inviscid flows. Without success we have attempted to satisfy the Neumann boundary conditions by linear extrapolation or adjusting the highest coefficient. This may be due to the insufficient accuracy of these two methods. Consequently the global coefficient adjustment method described in Part 1, is successfully applied to treat the Neumann boundary conditions for the present problem.

We first compare the resolutions for different grid numbers, where the free-stream Mach number and Reynolds number are set to four and 4000, respectively. The parameters for the cases with the collocation point numbers

TABLE III

Data for Different Cases

Mach number	Grid size	Time step Δt	Time step interval for filtering	Critical wave number
4	17×17	0.0008	2	9
4	33×33	0.00025	3	14
8	33×33	0.00008	3	10

$M = N = 16$ and 32 are shown in Table III. The critical wave number at $M_\infty = 4$ is 9 for $M = N = 16$, and 14 for $M = N = 32$, implying that about half of the terms have to be filtered. The time increment must be decreased from 0.0008 to 0.00025, as the number of collocation points is increased from 16 to 32. The non-linear change in the time increment is due to the non-uniform distribution of the Chebyshev–Gauss–Lobatto points, where the minimum grid interval is inversely proportional to the square of the number of collocation points.

The resulting velocity vectors for $M = N = 16$ and 32 are shown in Figs. 17 and 18, respectively. In both cases, the shock wave locations are almost the same and the velocity vectors are quite similar, where the velocity boundary layers are clearly captured. It is very convenient that the collocation points become fine at both boundaries, body and shock wave, because good resolution is required there.

In Figs. 19 and 20, the temperature distributions in the radial direction are illustrated, corresponding to the above two cases: the grid number $M = N = 16$ and 32. The three lines correspond to $\theta = 0°$, 40°, and 80°, respectively. Note

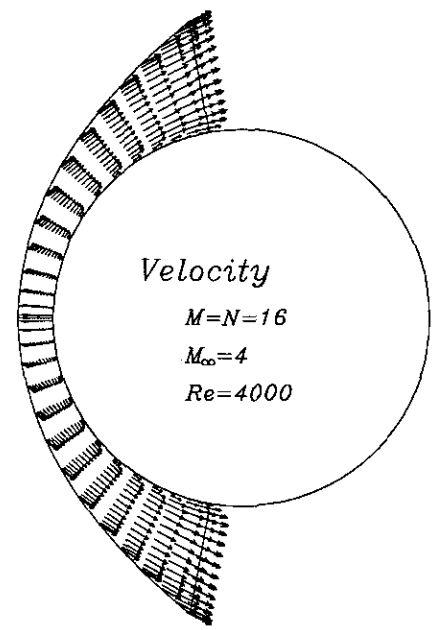

FIG. 17. Velocity vectors for $M = N = 16$, $M_\infty = 4$, and $\mathrm{Re} = 4000$.

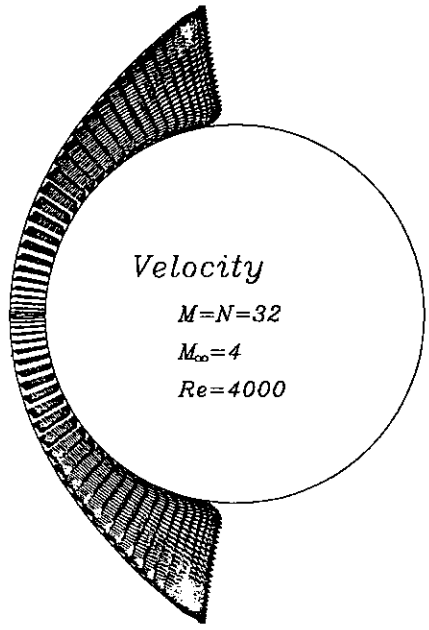

FIG. 18. Velocity vectors for $M = N = 32$, $M_\infty = 4$, and $\mathrm{Re} = 4000$.

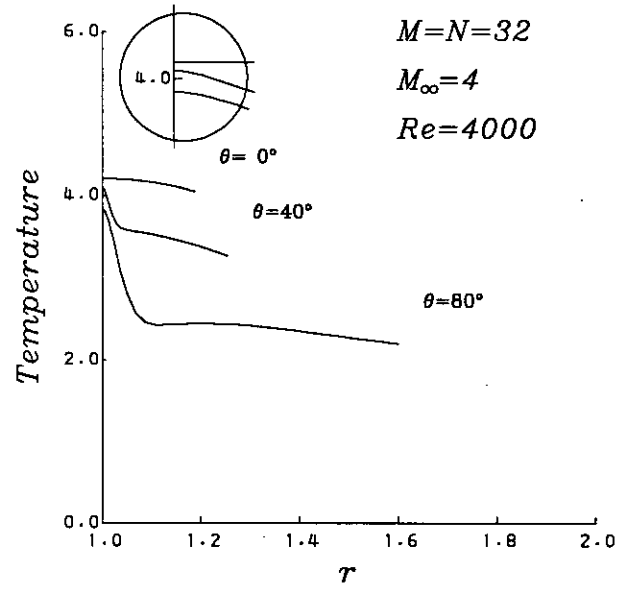

FIG. 20. Distributions of temperature along radius at these stations for $M = N = 32$, $M_\infty = 4$, and $\mathrm{Re} = 4000$.

that θ represents an angle from the upstream direction, which is different from the previous definition. The temperature increase near the wall is due to the thermal boundary layer under the adiabatic condition. The close-up figures are depicted in the circles by 10 times enlarging the scale of the abscissa. Although the results for the two different grid numbers have similar characteristics, the difference in each resolution is obvious.

Furthermore, let us examine the residuals for these two cases, which are illustrated in Figs. 21 and 22. The abscissa indicates the time-step number, and the ordinate indicates the maximum absolute residual of density on the logarithmic scale. The residual has a close relation with the filter, which affects the oscillation band and the convergence level of the residual. Since the filter is not performed at every time step, the non-linear waves are generated at the non-filtering steps. This is the reason for the oscillation band of the residual. If the coefficients are filtered more than the

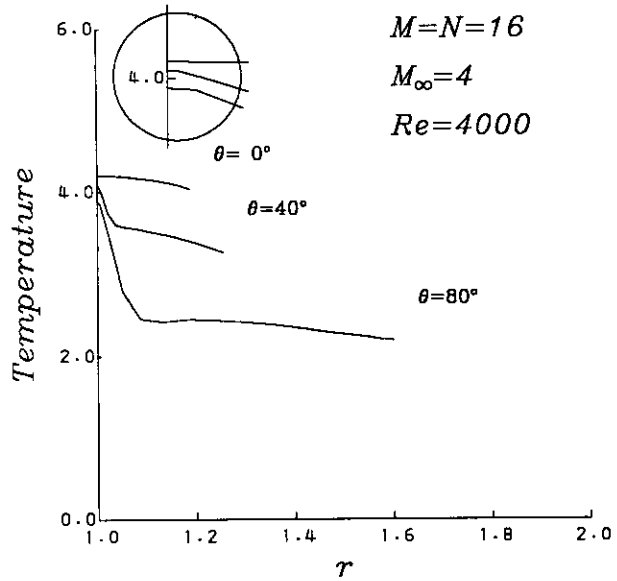

FIG. 19. Distributions of temperature along radius at these stations for $M = N = 16$, $M_\infty = 4$, and $\mathrm{Re} = 4000$.

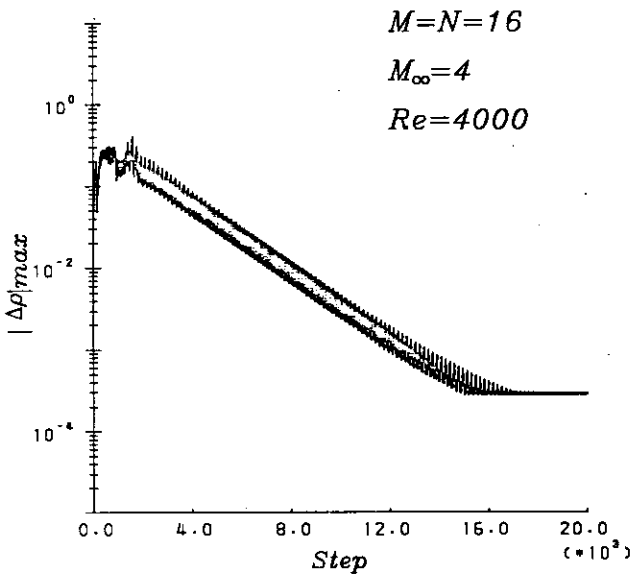

FIG. 21. Time history of maximum residual of density for $M = N = 16$, $M_\infty = 4$, and $\mathrm{Re} = 4000$.

TABLE IV

Comparison between SCM and FDM

Method	Absolute error of T_0(%)	CPU time (s)
SCM	0.18	274
FDM	0.37	37

magnitude of residual, the convergence process of the residual will be strongly influenced by filtering. An example for this is seen in Fig. 21, where the grid numbers are $M = N = 16$, and the critical wave number m_c is set to 9. In contrast, if the filtered coefficients are considerably small compared to the residual, the convergence process of the residual will be dominated by the unfiltered modes, and the convergence rate is faster than the former. This is seen in Fig. 22, where $M = N = 32$ and $m_c = 14$. The convergence level of the residual implies the balance between the stability due to filtering and the resolution determined by the number of collocation points. The converged residuals are about 3×10^{-4} and 5×10^{-5} for $N = 16$ and 32, respectively. This also demonstrates that the spectral accuracy is obtained in the present code.

Next we compare the present results with those by a finite difference code. The conditions between them are all the same except that the governing equations of the latter are axisymmetric Navier–Stokes equations transformed from Cartesian coordinates to generalized ones. Figures 23 and 24 show the Mach number contours of these two methods at $\mathrm{Re} = 4000$, $M_\infty = 4$, $M = N = 16$, respectively. Both the location of the shock wave and the contours are nearly the same, and we cannot judge which one is more accurate. The difference between them appears if we examine the data in detail. Table IV shows the absolute errors of the numerical results to the theoretical value for the stagnation temperature. The absolute error of the finite difference code is about two times larger than the present code. In the same table, the cpu times on the FA COM VP200 are also illustrated. Although the fast Fourier transform subroutine is modified for vectorization, the present code takes seven times as much cpu time as the finite difference code.

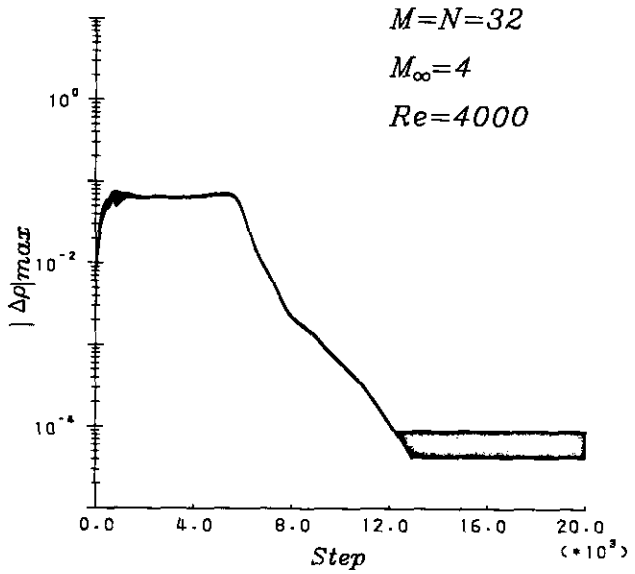

FIG. 22. Time history of maximum residual of density for $M = N = 32$, $M_\infty = 4$, and $\mathrm{Re} = 4000$.

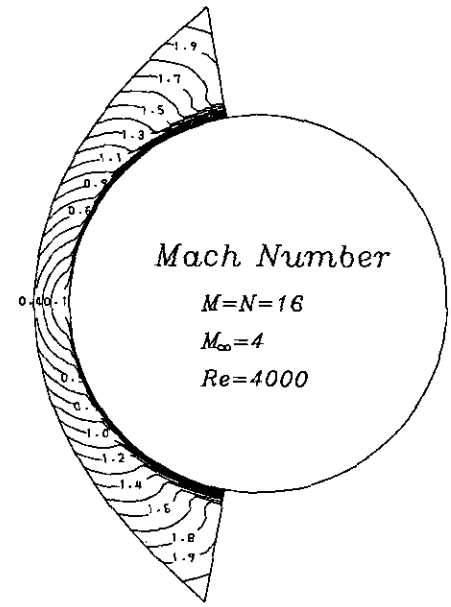

FIG. 23. Mach number contours for $M = N = 16$, $M_\infty = 4$, and $\mathrm{Re} = 4000$ by the spectral collocation method.

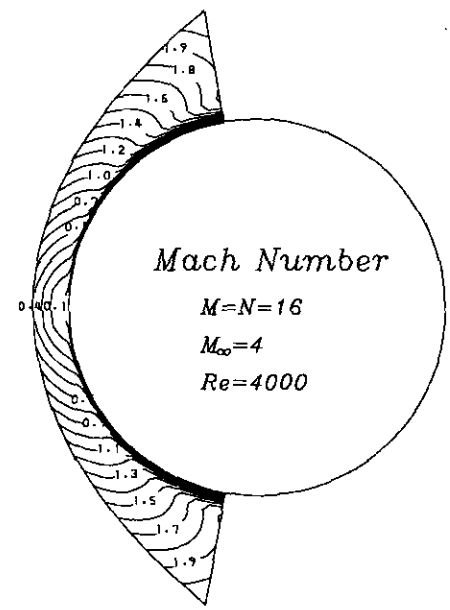

FIG. 24. Mach number contours for $M = N = 16$, $M_\infty = 4$, and $\mathrm{Re} = 4000$ by the finite difference method.

Finally, we make comparisons of the results of the spectral collocation code with the experimental data. We conducted an experiment for $M_\infty = 8$, using the shock tunnel at Nagoya University. The distribution of the pressure coefficient ratio is measured from the dynamic pressure along the body surface and the shock wave location is obtained from a Schlieren photograph. Furthermore, for comparison, an experimental data for $M_\infty = 4$ is taken from Ref. [19]. Figure 25 shows the distributions of the pressure coefficient ratio, $C_p/C_{p_{max}}$, where both calculations and experiments are included. The result of the modified Newtonian theory is also illustrated by a solid line. It is seen from the numerical results that the Mach number has almost no influence on the pressure coefficient ratio. This represents the Mach independence principle in the hypersonic flow. Except for a slight difference in the downstream at $M_\infty = 4$, the agreement between the numerical and experimental results is excellent. Moreover, the modified Newtonian theory provides a good approximation to other data in the region $0 \leqslant \theta \leqslant 60°$.

In Fig. 26, the shock wave locations for $M_\infty = 8$ obtained by the calculation and the experiment are compared. The difference between them becomes remarkable toward downstream, and the former is located in front of the latter. The reason for this is that the calculated displacement thickness of the boundary layer is considerably thicker than that of the experiment due to the difference in Reynolds number: 4000 for the former and 314,000 for the latter. It can be concluded that those two results have a marginal agreement, although detailed discrepancy is seen to be due to the difference in parameters.

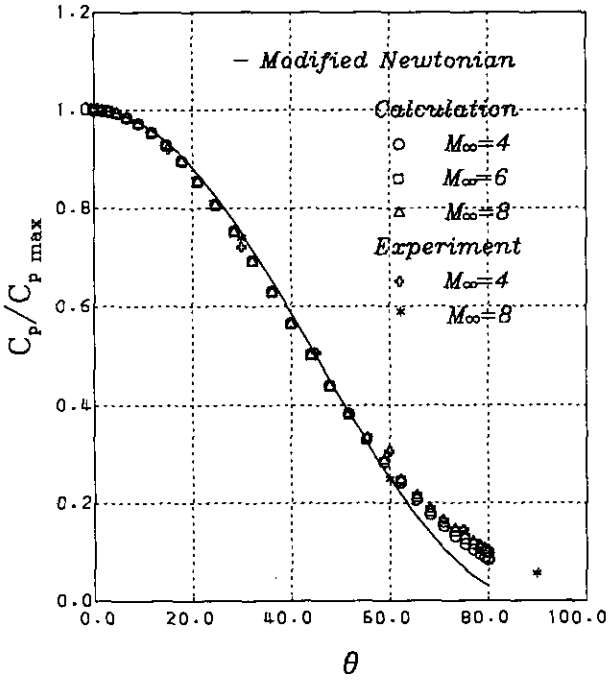

FIG. 25. Comparison of pressure coefficient ratio versus θ between modified Newtonian theory, numerical calculations, and experiments.

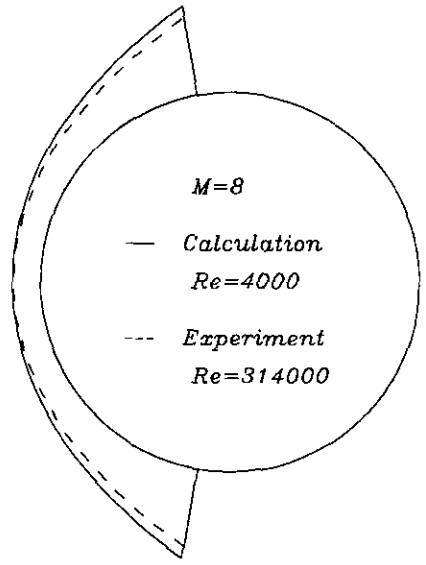

FIG. 26. Locations of bow shock wave at $M_\infty = 8$; calculation is at Re = 4000 and experiment is at Re = 314,000.

CONCLUDING REMARKS

The global coefficient adjustment method originated in the requirement of treating Neumann boundary conditions stably and accurately. Neither the extrapolation method nor the highest coefficient adjustment method lead to satisfactory results in complicated problems. The principle of a new technique proposed in the present study confines the influence of imposing the Neumann boundary condition to the neighborhood of a boundary in physical space. The derivation in Subsection 1.3 shows that all of the coefficients should be adjusted to meet this requirement. This is natural because the solution at any particular point is made up of all the spectral modes. Furthermore, since the global coefficient adjustment method is characterized by the spectral expansion, it is very stable and keeps the spectral accuracy.

The nonlinear property of viscous compressible flows makes it difficult to obtain good accuracy in a boundary layer. Therefore, we developed a compressible Navier–Stokes equations code for high-speed flows around a sphere by the spectral collocation method, where the global coefficient adjustment method was applied to treat Neumann conditions accurately. Comparisons between the results for two different numbers of collocation points show that the new technique works well and that spectral accuracy is also obtained. Good accuracy of the present code is also verified by comparing the result of the finite difference code with that of a shock tunnel experiment.

From the above-mentioned, the global coefficient adjustment method, which was verified to be effective in a fundamental test problem, it was also ensured to be useful in solving Navier–Stokes equations. Otherwise, any reliable solution will not be available for this problem by the spectral method.

REFERENCES

1. S. A. Orszag, *J. Fluid. Mech.* **50**, 689 (1971).
2. D. B. Haidvogel, *J. Comput. Phys.* **30**, 167 (1979).
3. S. A. Orszag, *J. Comput. Phys.* **37**, 70 (1980).
4. D. Gottlieb, M. Gunzburger, and E. Turkel, *SIAM J. Numer. Anal.* **19**, 671 (1982).
5. D. Gottlieb and L. Lustman, *SIAM J. Numer. Anal.* **20**, 909 (1983).
6. C. L. Street, T. A. Zang, and M. Y. Hussaini, *J. Comput. Phys.* **57**, 43 (1985).
7. M. Y. Hussaini, D. A. Kopriva, M. D. Salas, and T. A. Zang, *AIAA. J.* **23**, 234 (1985).
8. C. Canuto and A. Quarteroni, *J. Comput. Phys.* **71**, 100 (1987).
9. C. Canuto, *SIAM J. Numer. Anal.* **23**, 815 (1986).
10. A. T. Patera, *J. Comput. Phys.* **54**, 468 (1984).
11. M. Yasuhara, Y. Nakamura, and J. P. Wang, *J. Jpn Soc. Aerosp. Sci.* **36**, 542 (1988). [Japanese]
12. M. Yasuhara, Y. Nakamura, and J. P. Wang, in *Proceedings, 11th Int. Conf. on Numer. Methods in Fluid Dynamics, Williamsburg, VA, 1988*, edited by D. L. Dwoyer *et al.* (Springer-Verlag, Berlin, 1989), p. 607.
13. J. P. Wang, Y. Nakamura and M. Yasuhara, *J. Jpn Soc. Aerosp. Sci.* **38**, 232 (1990). [Japanese].
14. J. P. Wang, Y. Nakamura, and M. Yasuhara, in *Proceedings, Int. Sympos. Comput. Fluid Dynamics II, Nagoya, Japan, 1989*, edited by M. Yasuhara *et al.*, p. 1035.
15. D. A. Kopriva, T. A. Zang, and M. Y. Hussaini, *AIAA J.* **29**, 1458 (1991).
16. G. Moretti, *PIBALL Report* (New York, Polytechnic Institute of Brooklyn, 1968), p. 68.
17. M. Y. Hussaini, D. A. Kopriva, M. D. Salas, and T. A. Zang, *AIAA J.* **23**, 64 (1985).
18. K. J. Weimnenster and H. H. Hamilton II, NASA TP 2103, 1983 (unpublished).
19. R. S. Hickman and W. H. Giedt, *AIAA J.* **1**, 665 (1963).